The Influenza M2 Cytoplasmic Tail Changes the Proton-Exchange Equilibria and the Backbone Conformation of the Transmembrane Histidine Residue to Facilitate Proton Conduction

Shu Y. Liao, **Yu Yang**, **Daniel Tietze**[‡], and **Mei Hong**[*]

Department of Chemistry, Massachusetts Institute of Technology, Cambridge, MA 02139

Abstract

The influenza M2 protein forms an acid-activated tetrameric proton channel important for the virus lifecycle. Residue His37 in the transmembrane domain is responsible for channel activation and proton selectivity. While the structure and dynamics of His37 have been well studied in TM peptide constructs, it has not been investigated in the presence of the full cytoplasmic domain, which increases the proton conductivity by 2-fold compared to the TM peptide. We report here ^{13}C and ^{15}N chemical shifts of His37 in the cytoplasmic-containing M2(21-97), and show that cationic histidines are already present at neutral pH, in contrast to the TM peptide, indicating that the cytoplasmic domain shifts the protonation equilibria. Quantification of the imidazole ^{15}N intensities yielded two resolved proton dissociation constants (pK_a's) of 7.1 and 5.4, which differ from the TM result but resemble the M2(18–60) result, suggesting cooperative proton binding. The average His37 pK_a is higher for M2(21–97) than for the shorter constructs. We attribute this higher pK_a to direct and indirect effects of the cytoplasmic domain, which is rich in acidic residues. 2D ^{13}C-^{13}C correlation spectra reveal seven His37 Cα-Cβ cross peaks at different pH, some of which are unique to the cytoplasmic-containing M2 and correspond to more ideal α-helical conformations. Based on the pH at which these chemical shifts appear and their sidechain structures, we assign these conformations to His37 in differently charged tetramers. Thus, the cytoplasmic domain facilitates proton conduction through the transmembrane pore by modifying the His37-water proton-exchange equilibria and the His37 backbone conformational distribution.

Introduction

The 97-residue M2 protein of the influenza A virus forms a homo-tetrameric proton channel that is essential for virus infection and replication [1–5]. The protein contains three domains: a highly conserved N-terminal ectodomain (residues 1–21)[6], an α-helical transmembrane (TM) domain (residues 22–46), and a cytoplasmic domain (residues 47–97). The

[*]Corresponding Author: Mei Hong, Tel: 617-253-5521, meihong@mit.edu.
[‡]Current address: Eduard-Zintl-Institute of Inorganic and Physical Chemistry, Technische Universität Darmstadt, Alarich-Weiss-Straäe 8, 64287 Darmstadt, Germany

cytoplasmic domain contains an amphipathic helix (AH) [7] spanning residues 46 to 62, followed by a C-terminal tail [6,8]. The proton channel opens when the ectodomain is exposed to low pH of the external environment. After virus endocytosis, the acidic endosome activates the M2 channel, which acidifies the virion, causing uncoating of the ribonucleoprotein and release of the viral genetic content to the host cell [9]. In a later stage of the virus lifecycle, the proton channel activity prevents premature conformational changes of hemagglutinin. The acid activation and proton selectivity of M2 are controlled by a single residue, His37, in the TM domain [10,11].

Extensive electrophysiological experiments, molecular dynamics simulations, X-ray crystallography and NMR studies have been conducted to elucidate how M2 conducts protons (for recent reviews, see [12,13]). Three proton conduction mechanisms have been proposed: a water-wire model [14–16], a shuttle model [17,18], and a strong hydrogen-bond model [7,19]. Solid-state NMR data of phospholipid-bound TM peptide (M2TM) provided compelling evidence for the shuttle mechanism. These data showed that the His37 imidazole ring undergoes microsecond reorientations and proton exchange with water only at acidic pH [17,20,21]. At pH 5.4, a proton exchange rate of 4.5×10^5 s^{-1} was determined for wild-type M2TM based on the observed ^{15}N exchange peaks between neutral and cationic histidines [17]. S31N mutation in the TM domain significantly increases the exchange rates, as seen by the much narrower linewidths of the chemical-exchange peaks [22]. Based on the relative concentrations of cationic and neutral histidines detected in ^{15}N NMR spectra, the four pK_a's of the His37 tetrad in membrane-bound M2TM have been determined and are found to depend on the membrane composition. In DMPC/DMPG bilayers, the pK_a's are 8.2, 8.2, 6.3, and < 5.0 [19], while in a cholesterol-containing virus-mimetic membrane, the pK_a's decrease to 7.6, 6.8, 4.9, and 4.2 [17]. Both sets of pK_a values, when considered in the context of pH-dependent proton currents [10], indicate that the +3 charged state of the channel is responsible for the majority of the proton conductivity.

While these studies provided detailed insights into the proton conduction mechanism of the M2 channel, a significant question remains as to whether the His37 structure and dynamics measured in the TM peptide accurately reflects the situation in the full-length protein. Although the TM domain is the heart of the proton channel, the conductivity of M2TM is about half of the conductivity of full-length M2 (M2FL) [23]. The minimal construct that reproduces M2FL's activity includes both the TM and AH domains, a construct that has been called the conductance domain (M2CD). Mutation of Lys49 in the AH abolishes the channel activity [24]. Various truncation mutants in the cytoplasmic tail that is C-terminal to the AH have also been reported to impair proton conductance [25], suggesting that the tail also affects the channel activity. Thus, it is important to determine whether the conformation, dynamics, and charged-state distribution of His37 in a fully functional channel are the same as in the TM peptide. In addition, a recent structural study of M2FL using chemical-shift prediction and spectral simulations suggested that the cytoplasmic tail is intrinsically disordered [6]. This result raises the question as to how an unstructured segment might regulate proton conduction through the TM pore.

Several studies of M2CD and M2FL involving the His37 chemical shifts have been recently reported [7,26–30]. Interestingly, these chemical shifts show non-negligible differences even at

similar pH. The origin for these differences is not yet understood: they could result from lipid membrane differences, sample preparation differences, or real structural differences caused by the extra-membrane domains. Extensive peak doubling was detected for one of the M2CD constructs [26], indicating breaking of the tetramer's C_4 symmetry and a dimer-of-dimer topology. This peak doubling was observed at pH 7.8, thus it cannot be interpreted by an imidazole-imidazolium dimer model proposed for His37 at acidic pH [29]. A study of M2(18–60) bound to the DPhPC membrane quantified the His37 pK_a's and found two distinct values, 7.53 and 4.52 [28], which differ from the His37 pK_a's in the TM peptide. Thus, the pH chemistry and structure of His37 in longer M2 constructs are still unresolved.

To elucidate the His37 structure in fully functional M2, we have now expressed and purified M2(21–97). The N-terminal ectodomain is skipped at present, to allow sufficient single-site sensitivity in the NMR spectra and because the ectodomain has not been implicated in the proton-channel activity [23]. We measured the ^{13}C and ^{15}N chemical shifts of His37 in M2(21–97) bound to a virus-envelope-mimetic lipid membrane [22,31]. We show that in the presence of the full cytoplasmic domain, His37 protonates at higher pH than M2TM [17] and M2CD [28]. The His37 pK_a's in M2(21–97) are distinct from those of M2TM but have qualitative similarities to those of M2CD, in that 2 instead of 4 pK_a's are resolved, suggesting cooperative proton binding. In addition to the sidechain structure, 2D ^{13}C-^{13}C correlation spectra revealed complex, pH-dependent Cα and Cβ chemical shifts, which can be assigned to His37 conformations in differently charged tetrads. These results give detailed insights into how the cytoplasmic tail fine-tunes the His37 sidechain chemistry, backbone conformation, and the assembly of the four-helix bundle.

Material and Methods

Expression, purification and isotopic labeling of M2(21–97)

The cDNA of M2(21-97) from influenza A H3N2 virus, modified by adding an N-terminal His-tag and a TEV protease cleavage site, was inserted into plasmid pET21. His57 and His90 were mutated to glutamine to make residue 37 the only histidine in the protein. The amino acid sequence of M2(21–97) is shown in Fig. 1, where the first three residues, SNA, are the remnant of the His-tag after cleavage by TEV protease. Most M2 samples are ^{13}C, ^{15}N-labeled only at His37, except for the DMPC-bound protein, which includes ^{13}C, ^{15}N-labeled His, Ala, Gly and Ser to allow the investigation of the overall conformation of the protein.

E. coli cells were cultured on ampicilin-containing Lysogeny broth (LB) agar. A fresh colony was used to inoculate 100 ml of LB media. The cells were grown in a shaker incubator overnight at 37°C. A 10 ml aliquot was used to inoculate 1 L of LB media until OD_{600} reached 0.7–0.8. The cells were spun down (20°C, 7000 rpm, 10 min) and resuspended in 500 mL M9 media (48 mM Na_2HPO_4, 22 mM KH_2PO_4, 8.55 mM NaCl, 1g/L NH_4Cl, 4 g/L glucose, 2 ml/L of 1 M $MgSO_4$, 0.1 ml/L of 1 M $CaCl_2$, 100 mg/ml ampicilin). After half an hour, the temperature was decreased to 25°C and uniformly ^{13}C, ^{15}N-labeled amino acids were added. For VM+ bound M2(21–97), ^{13}C, ^{15}N-labeled His was added at 100 mg/L. For DMPC-bound M2, ^{13}C, ^{15}N-labeled His, Ala, Gly were added at 100 mg/L while unlabeled Leu, Ile, Val, Lys and Arg were added at 50 mg/L

to minimize scrambling. This sample showed Ser signals in addition to the ^{13}C signals of the labeled amino acids, suggesting scrambling from Gly to Ser [32,33]; however, the scrambling does not affect conformational analysis of the protein. Concurrent to the addition of the amino acids, 0.1 mM isopropyl β-D-thiogalactopyranoside (IPTG) was added to induce protein expression. The cells were grown for 18 h, then resuspended in the lysis buffer (50 mM Tris-HCl, 50 mM NaCl).

Cells were sonicated using a probe sonicator at power level of 3.5 on ice 5 seconds on and 5 seconds off for 9 cycles, then benzonase nuclease and phenylmethylsulphonyl fluoride were added to degrade nucleic acids and inhibit proteases, respectively. After incubation for 30 min at 4°C, cells were sonicated again for 1 hour to break open the cell wall. The soluble fraction, which contains nucleic acids, cytoplasmic proteins and small molecules, was removed by centrifugation (10,000 × g, 8°C, 30 min). The insoluble fraction, which consists of M2-containing inclusion bodies, other insoluble proteins and cell walls, was suspended in a lysis buffer with 6 M urea and 2% octyl-β-D-glucopyranoside (OG). After the suspension was shaken for 2 hours, the cell wall was removed by centrifugation at 10,000 × g and 8°C for 30 min, while the supernatant containing His-tagged M2(21–97) and other proteins was added to a Ni-NTA affinity column and placed on a Thermo Scientific Rocker at 4°C overnight to allow binding. 100 ml of wash buffer I (50 mM pH 7.8 Tris-HCl, 100 mM NaCl, 20 mM imidazole, 4 M urea, 1% OG) and 50 ml of wash buffer II (50 mM Tris-HCl, 100 mM NaCl, 20 mM imidazole, 2 M urea, 1% OG) were used to wash the column. Subsequently, 50 ml of refold buffer I (50 mM Tris-HCl, 100 mM NaCl, 20 mM imidazole, 0.5% OG, 20% glycerol) and 100 ml of refold buffer II (50 mM Tris-HCl, 50 mM NaCl, 0.5% OG, 20% glycerol) were applied to the column to refold the protein. Finally, 50 ml of elution buffer (50 mM pH 7.8 Tris-HCl, 50 mM NaCl, 300 mM imidazole, 0.5% OG, 20% glycerol) was used to elute M2(21–97) from the column. The amount of the protein was quantified from OD_{280} with an extinction coefficient of 9530 M^{-1} cm^{-1}. A monomer band of His-tagged M2(21–97) appears at 15 kDa on the SDS-PAGE gel (Fig. S1). About 16 mg M2 was obtained from 1 L of culture.

His-tag cleavage and purification of M2(21–97)

The His-tagged M2(21-97) was concentrated using an Amicon ultracentrifuge filter with a molecular weight cutoff of 3000 Da. The His-tag was cleaved using 1 : 5 mass ratio of TEV protease and M2. The completeness of digestion was monitored by analytical reversed-phase HPLC using a Vydac C4 column (5 μm particle size, 0.46 cm x 15 cm) were used, and a gradient of 20–99% acetonitrile containing 0.1% trifluoroacetic acid for 25 minutes at 1.5 mL/ min (Fig. S2). The molecular weight of the cleaved M2(21–97) was confirmed by electrospray ionization mass spectrometry (ESI-MS) (Fig. S3).

His37-labeled M2(21–97) was purified by preparative HPLC using a Vydac C4 column (10 μm particle size, 2.2 cm x 25 cm) with a gradient of 35–99% acetonitrile for 70 min at a flow rate of 10 mL/ min. The protein fraction was lyophilized to obtain pure M2(21–97). About 12 mg protein was obtained per liter, indicating a cleavage yield of ~75%. The His, Ala, Gly and Ser-labeled M2(21–97) was purified by Ni affinity column chromatography, and the purity of the eluted fraction was verified by analytical HPLC.

Membrane reconstitution of M2(21–97)

All His37-labeled M2(21–97) samples were reconstituted into the VM+ membrane, which contains 1-palmitoyl-2-oleoyl-sn-glycero-3-phophocholine (POPC), 1-palmitoyl-2-oleoyl-sn-glycero-3-phosphoethanolamine (POPE), egg sphingomyelin (SM) and cholesterol (Chol) at molar ratios of 25.6% : 25.6% : 25.6% : 23% [31]. This membrane mimics the virus envelope lipid composition, and the presence of cholesterol and SM immobilizes the whole-body uniaxial rotational diffusion of M2 so that protein internal dynamics can be investigated at physiological temperature [34]. POPC, POPE and cholesterol were dissolved in chloroform, while SM was dissolved in a chloroform/methanol mixture. The solutions were mixed and the solvent was removed by nitrogen gas. The lipid film was redissolved in a small amount of cyclohexane and lyophilized overnight. The resulting homogeneous lipid powder was re-suspended in 1 ml of 10 mM buffer of the desired pH, vortexed, and subject to eight freeze-thaw cycles between liquid nitrogen temperature and 37–45°C to create large unilamellar vesicles. About 10 mg of protein was solubilized in 1 ml of buffer using a minimum amount of OG (< 40 mg). The lipid vesicles were added to the M2(21–97) solution, then the solution was diluted with 2–5 ml buffer to reduce the OG content to below the critical micelle concentration. The proteoliposome solution was vortexed for 2 hours and dialyzed against 1 L buffer at room temperature for 3 days with six buffer changes. The dialyzed proteoliposomes were spun down at 55,000 rpm for 4 hours using a SW60 Ti rotor (Beckman Instruments), then the membrane pellets were transferred into 4 mm magic-angle-spinning (MAS) rotors. The protein : lipid molar ratio of His37-labeled samples was 1 : 22.5. Most samples contained 8–10 mg protein, the requisite amount of lipids and ~40 wt% water.

Five VM+ bound His37-M2(21–97) samples were prepared at pH 7.5, 7.0, 6.5, 6.1 and 5.4. To ensure that His37 was exposed to the appropriate pH from the beginning, the protein-detergent solution and the lipid vesicle solution were pH-controlled before mixing. In our experience, if the pH was adjusted to the desired value only after protein-lipid mixing, then the His37 structure retains "memory" of the pH of the first solution to which it was exposed. The pH 7.5, 7.0 and 6.5 samples were prepared using 10 mM Tris, HEPES and Bis-Tris buffers, respectively, while the pH 6.1 and pH 5.4 samples were prepared using a 10 mM citrate buffer. All buffers also contain 1 mM EDTA and 0.01 mM NaN$_3$. His, Ala, Gly and Ser-labeled M2(21–97) was reconstituted into DMPC bilayers in a similar fashion at pH 7.0 using the HEPES buffer and a protein : lipid molar ratio of 1 : 15.

Solid-state NMR spectroscopy

Solid-state NMR spectra were measured on Bruker spectrometers at ^{1}H Larmor frequencies of 400 MHz (9.4 Tesla), 600 MHz (14.1 Tesla), and 900 MHz (21.1 Tesla). 4 mm and 3.2 mm MAS probes were used. All ^{13}C chemical shifts were referenced externally to the adamantane CH$_2$ chemical shift at 38.48 ppm on the TMS scale [35]. ^{15}N chemical shifts were referenced to the ^{15}N peak of N-acetylvaline at 122.0 ppm on the liquid ammonia scale [36]. Sample temperatures are thermocouple-reported values.

1D ^{13}C and ^{15}N cross-polarization (CP) spectra were measured under 7–16 kHz MAS at 308 K and 243 K. The high-temperature spectra detect conformational dynamics and proton

exchange dynamics, while the low-temperature spectra provide information on the rigid-limit tautomeric structure and protonation state of His37. 1D ^{13}C double-quantum (DQ) filtered spectra were measured to suppress the natural-abundance lipid ^{13}C signals and give protein-only ^{13}C spectra. The SPC5 sequence was used for ^{13}C-^{13}C dipolar recoupling [37]. The measured dipolar recoupling efficiency was 10–20% at the MAS frequency of 7 kHz. 2D ^{13}C-^{13}C DARR correlation spectra [38] of VM+ bound M2(21-97) were measured at 600 MHz using mixing times of 30 – 40 ms between 243 K and 249 K. 2D ^{13}C-^{13}C PDSD spectra of DMPC-bound M2(21–97) were measured at 253 K using a 100 ms mixing time on the 900 MHz spectrometer.

Results

pH-dependent structure of His37 in M2(21–97)

We investigate the His37 structure in VM+ bound M2(21–97) through ^{13}C and ^{15}N chemical shifts. The pH- and tautomer-dependent chemical shifts of histidine are well known from small-molecule studies [39,40] as well as previous M2TM data [21,22], with several characteristic chemical shifts serving as fingerprints of the imidazole structure. The Cδ2 chemical shift is 113–114 ppm for the Nε2-protonated τ tautomer, 124–125 ppm for the Nδ1-protonated π tautomer, and 116–119 ppm for cationic histidine (Fig. 2a). The Cγ chemical shift is also resolved among the three states, adopting the most downfield values (136–138 ppm) for the τ tautomer, the most upfield values (126–129 ppm) for the π tautomer, and intermediate values (129– 132 ppm) for cationic histidine. Using the Cγ and Cδ2 chemical shift difference as a criterion, the τ and π tautomers are distinguished by large (> 20 ppm) and small (< 5 ppm) chemical shift differences, respectively, while cationic histidine has intermediate chemical shift difference of 10–15 ppm [41].

Fig. 2 shows the 1D ^{13}C CP-MAS spectra of His37 as a function of pH. At pH 7.5 and 243 K, where conformational motion and proton exchange are largely frozen, the ^{13}C spectra show Cδ2 chemical shifts for both neutral tautomers, but in addition, a small cationic Cδ2 peak at 117 ppm is also observed. With decreasing pH, the cationic Cδ2 and Cγ signals increase in intensity, as expected for the increased cationic histidine population. Since lipid double-bond ^{13}C and cholesterol carbons of the virus-mimetic membrane resonate at 130, 131 and 134 ppm, which partially overlap with the imidazole Cγ and Cε1 signals, we conducted a DQ filtered ^{13}C experiment to suppress these lipid natural-abundance ^{13}C signals. The DQ filtered spectra of the pH 7.5 sample (Fig. 3a) show that the 117-ppm peak survives, confirming that a small population of His37 is already protonated at pH 7.5. At pH 5.4, the DQ filtered spectrum shows a prominent cationic Cγ peak at 129 ppm (Fig. 3b), without overlap from the lipid signals. Moreover, the τ tautomer Cε1 peak is much weaker than at pH 7.5, indicating reduced neutral histidine content.

The DQ filtered ^{13}C spectra also show multiple Cα and Cβ signals at both pH 7.5 and pH 5.4, signifying multiple backbone conformations. The pH 7.5 spectrum resolves three Cα peaks while the pH 5.4 spectrum shows two main Cα peaks. The center of gravity of the Cα signals at high pH is shifted to smaller chemical shifts (upfield) compared to the low-pH spectrum, while the Cβ chemical shifts exhibit the opposite trend. Since smaller Cα and

larger Cβ chemical shifts correspond to less ideal α-helical conformations, these differences indicate that the His37 (φ, ψ) torsion angles are less helical at high pH than at low pH.

To understand the origin of the multiple His37 Cα and Cβ chemical shifts and the corresponding conformations, we measured 2D ^{13}C-^{13}C correlation spectra of M2(21–97) as a function of pH and compared them with the M2TM spectra at similar pH and membrane composition (Fig. 4) [17,21]. At pH 7.5, two prominent (Cα, Cβ) cross peaks are resolved in the M2(21–97) spectra. The (55, 30) ppm and (55, 28) ppm peaks can be assigned to τ and π tautomers based on their connectivities to the imidazole Cγ, Cδ2 and Cε1 peaks (Table 1). These chemical shifts are identical to those observed in wild-type M2(22–46) [17] and S31N M2(19–49) [22] at high pH, indicating that the cytoplasmic domain does not perturb the backbone conformations of the neutral tautomers.

In addition to the neutral tautomer peaks, five more (Cα, Cβ) cross peaks are observed in the M2(21–97) spectra at varying pH. We denote these cross peaks as cat0, cat1, cat3 and cat4, and deduce their structures based on their correlations with the imidazole chemical shifts. The cat0 cross peak is observed only in the pH 7.0 spectrum of DMPC-bound M2(21–97) and has (Cα, Cβ) chemical shifts of (60, 30) ppm. It is correlated with a Cδ2 chemical shift of 114 ppm, which is diagnostic of a neutral τ tautomer. Interestingly, the τ tautomer in all other M2 samples studied so far shows non-ideal α-helical chemical shifts of 55 and 30 ppm, while the cat0 chemical shifts correspond to an ideal helical conformation. Thus, the combination of the cytoplasmic domain and a non-cholesterol membrane induces a τ tautomer with an ideal α-helical backbone.

The cat1 cross peak, at (Cα, Cβ) chemical shifts of (58, 29) ppm, is found in the pH 7.5 and 7.0 spectra of VM+ and DMPC-bound M2(21–97) (Fig. 4a, b). This peak correlates with Cγ, Cδ2 and Cε1 chemical shifts of 133, 117 and 134 ppm (Table 1), which is diagnostic of cationic histidine. Thus, the cat1 backbone is associated with a cationic imidazolium sidechain.

The pH 5.4 spectrum of M2(21–97) shows three broad and partially overlapped (Cα, Cβ) cross peaks, indicating that low pH induces larger conformational distributions of the His37 backbone. The dominant peak, cat3, appears at (Cα, Cβ) chemical shifts of (58, 26) ppm, and is weakly present in the pH 5.2 spectrum of M2(22–46) (Fig. 4c, e). This peak correlates with aromatic chemical shifts of 129, 118 and 136 ppm, which indicate a classical imidazolium. A cat4 peak at (60, 29) ppm is also correlated with a cationic sidechain, but this peak has not been observed in M2TM spectra. Finally, a cat2 cross peak with less helical (Cα, Cβ) chemical shifts of (55, 29) ppm is well resolved in the M2TM spectrum but significantly overlaps with the cat3 peak in the M2(21–97) spectrum. The cat2 Cα/Cβ chemical shifts are similar to those of the neutral τ tautomer, but its correlated Cδ2 chemical shift of 118 ppm reveals the sidechain to be cationic.

Based on the chemical shift correlations, the pH at which the cross peaks are observed, the known pK_a's of M2TM [17], as well as the measured pK_a's of M2(21–97) below, we can unambiguously assign the cat2 and cat3 states to cationic histidines in the +2 and +3 tetrads of both short and long M2 constructs. We tentatively assign the cat4 state to cationic

histidines in the +4 tetrad (see below), while the cat0 and cat1 conformations most likely correspond to neutral and cationic histidines in low charged tetrads in M2(21–97) (Table 1). The fact that the cat3 signal is much stronger in M2(21–97) than M2TM at similar pH indicates that the cytoplasmic domain facilitates His37 protonation, while the relatively ideal helical chemical shifts of cat0 and cat1 indicates that the cytoplasmic domain increases the His37 α-helicity.

To determine whether the conformational polymorphism indicated by these chemical shifts is specific to His37 or a general property of the protein, we examined the Ala, Ser and Gly chemical shifts of DMPC-bound M2(21–97). The protein contains 4 Ala, 4 Gly, and 9 Ser residues. However, only two Ala Cα-Cβ cross peaks are observed (Fig. 5): the dominant peak appears at α-helical chemical shifts that match those of Ala29 and Ala30 in M2TM [34,42], while the minor peak appears at random-coil chemical shifts that have been observed in the J-INADEQUATE spectrum of full-length M2, and has been assigned to Ala83 and Ala86 [6]. Thus, there is no general conformational polymorphism for the whole protein. This differs from the extensive peak doubling seen in M2(18–60) [26], suggesting that the latter may result from different sample preparation procedures used in the protein expression, purification and membrane reconstitution, although we cannot rule out a real structural effect specific to M2(18–60), which lacks the cytoplasmic tail.

^{15}N chemical shifts and pK$_a$'s of His37 in M2(21–97)

To obtain more quantitative information about the effect of the cytoplasmic domain on the His37-water proton exchange equilibria, we measured the ^{15}N spectra of His37 from pH 7.5 to 5.4 (Fig. 6) and compared them with the M2TM spectra (Fig. 7). Histidine aromatic ^{15}N chemical shifts are highly sensitive to the protonation state and tautomeric structure. Unprotonated nitrogens in neutral histidine exhibit an ^{15}N chemical shift of 250 ppm, while protonated nitrogens exhibit chemical shifts of 160 – 190 ppm (Fig. 2a). Protonation and deprotonation on the sub-microsecond timescale average the ^{15}N chemical shifts. By measuring the pH dependence of the ^{15}N chemical shifts, we probe the protonation equilibria of His37. By comparing the spectra at low and high temperature, we discern conformational dynamics and proton-exchange kinetics.

At pH 7.5, His37 exhibits a strong 250-ppm peak (Fig. 6a), indicating the expected high concentration of neutral histidines. The protonated Nε2 peak of the τ tautomer and Nδ1 peak of the π tautomer resonate at 159 ppm and 168 ppm, respectively, similar to the M2TM chemical shifts. An additional 175-ppm peak, which has been assigned to cationic histidine in M2TM, is also detected, consistent with the ^{13}C result that some of the His37 residues in this construct are protonated already at pH 7.5. Lowering the pH reduced the unprotonated ^{15}N intensity while increasing the 175-ppm and 170-ppm intensities of cationic histidine, as expected, but the intensity change is more drastic than that of M2TM. At pH 5.4, the M2(21–97) spectra resemble the pH 4.5 spectra of the TM peptide [17], with a broad and prominent ^{15}N peak at 175 ppm. This supports the conclusion that the cytoplasmic tail shifts the His37 equilibrium to the protonated state. At low pH, the ^{15}N linewidths of the protonated ^{15}N peaks are broader than at high pH, with intensities extending to ~190 ppm. The line broadening is more pronounced at high temperature.

However, unlike the TM peptide, no resolved exchange peak is observed for M2(21–97) between pH 6 and 5 (Fig. 7a–c).

We previously extracted the proton dissociation constants, pK_a's, of the His37 tetrad in M2TM from the intensity ratios, I_{NH}/I_N, of the protonated and unprotonated imidazole ^{15}N peaks as a function of pH [17]. The relative concentrations of neutral and cationic histidines depend on I_{NH}/I_N according to

$$[His]/[HisH^+] = \frac{2}{(I_{NH}/I_N)/\kappa - 1} \quad (1)$$

where κ is a parameter that accounts for the lower CP efficiency of unprotonated ^{15}N than protonated NH. The histidine concentration ratios depend on the four pK_a's according to [17,19]

$$\frac{[His]}{[HisH^+]} = \frac{1 + \frac{K_{a1}}{10^{-pH}} + 2 \cdot \frac{K_{a1} \cdot K_{a2}}{10^{-2pH}} + 3 \cdot \frac{K_{a1} \cdot K_{a2} \cdot K_{a3}}{10^{-3pH}} + 4 \cdot \frac{K_{a1} \cdot K_{a2} \cdot K_{a3} \cdot K_{a4}}{10^{-4pH}}}{4 + 3 \cdot \frac{K_{a1}}{10^{-pH}} + 2 \cdot \frac{K_{a1} \cdot K_{a2}}{10^{-2pH}} + 1 \cdot \frac{K_{a1} \cdot K_{a2} \cdot K_{a3}}{10^{-3pH}}}, \quad (2)$$

where pK_{a4} is the highest pK_a of the first protonation reaction while pK_{a1} is the lowest pK_a for the fourth protonation reaction.

Using this approach, we extracted the pK_a's of His37 in M2(21–97). The ^{15}N intensities of the pH 6.5 sample (data not shown) are anomalous and inconsistent with the other spectra, thus we did not include this data. Table 2 lists the I_{NH}/I_N values and the resulting $[His]$ / $[HisH^+]$ obtained using measured κ values of 1.3–1.6. Interestingly, the only satisfactory fit to the $[His]$ / $[HisH^+]$ ratios consists of two distinct pK_a's, at 7.1 and 5.4 (Fig. 8a). No physically reasonable fits are obtained using three or four independent pK_a's.

Discussion

The cytoplasmic domain facilitates His37 protonation and increases the pK_a's

The His37 ^{13}C and ^{15}N chemical shifts in M2(21–97) indicate that the cytoplasmic domain increases the proton-channel activity of M2 by facilitating His37 protonation. Multiple cationic histidine signals are detected at pH 7.5 in M2(21–97), which were not observed before in M2TM at similar pH [17,22]. These include the 175-ppm ^{15}N peak, the 118-ppm Cδ2 peak, the 129-ppm Cγ peak, and the cat1 (Cα, Cβ) cross peak in the 2D ^{13}C–^{13}C correlation spectrum. In addition, the high-temperature ^{15}N spectra show larger linewidths than M2TM, suggesting that dynamic events such as proton exchange, ring reorientation [21] and tautomerization [22], which occur at lower pH in M2TM, are more pronounced in the cytoplasmic-containing M2.

Based on the pH-dependent ^{15}N intensities, we resolved two pK_a's, 7.1 and 5.4, for His37 in M2(21–97), which differ from the His37 pK_a's in shorter M2 constructs (Table 3). The average pK_a (6.3) of His37 in M2(21–97) is 0.4 pH unit higher than the average pK_a of M2TM in a similar cholesterol-containing lipid membrane [17], consistent with the

cytoplasmic domain's ability to facilitate His37 protonation. It is also slightly higher than the average pK_a in M2(18–60) [28]. Since M2(18–60) was investigated in the highly fluid DPhPC membrane, which is expected to facilitate proton binding, the true difference in the protonation equilibrium between M2(21–97) and M2(18–60) may be even larger, suggesting that the post-AH cytoplasmic tail is independently able to promote His37 protonation. Interestingly, both M2(18–60) and M2(21–97) yielded only two resolved pK_a's, in qualitative difference from M2TM, suggesting that protonation is more cooperative in the presence of part or the whole of the cytoplasmic domain. This cooperativity can be visualized in the charged tetrad distribution as a function of pH (Fig. 8b): both the +1 and the +3 tetrads have depressed populations than those of M2TM (Fig. 8c), indicating the increased likelihood of simultaneous binding of two protons by the neutral channel and the +2 channel.

How does the cytoplasmic domain facilitate His37 protonation? An examination of the amino acid sequence shows that this domain contains ten highly conserved acidic Glu and Asp residues but only seven basic Arg and Lys residues (Fig. 1, S4). As a result, the isoelectric point for this domain is 4.6, which means that at pH 5.4, the cytoplasmic domain has a net charge of −3.0 per monomer or −12.0 per tetramer. We suggest that this negative charge may provide an electrostatic driving force for protons from the N-terminal side of the protein to associate with His37. Alternatively or in addition, the electrostatic repulsion among the four negatively charged cytoplasmic domains may increase the tilt angle of the TM helices and widen the pore, thus increasing the proton transfer rates (Fig. 9). Such pore widening has been observed in BK channels, where eight conserved anionic residues at the C-terminus double the K^+ conductance [43]. The potential importance of the large number of acidic residues in the cytoplasmic domain does not contradict the functional relevance of the isolated basic residue Lys49 [24]: the former is a non-specific electrostatic effect, while the exact mechanism of Lys49's influence on proton conduction is not yet known, and may involve site-specific effects such as intermolecular contacts between Lys49 and other residues.

The acidic nature of the cytoplasmic domain may also partly account for the increased cooperativity of proton binding and the higher populations of the even-charged states: by increasing the separation among the four histidines through electrostatic repulsion among the four cytoplasmic domains, the even charged state of +2 may be favored over the +1 tetrad due to increased possibility of histidine interaction with water, while the +4 channel is also less energetically unfavorable than +3 compared to the situation in M2TM.

The tetrad populations deduced from the pK_a's allow us to estimate the relative single-channel time-averaged conductivities of the different charged tetrads, using a similar approach as shown before [17]. We find that the +2, +3 and +4 channels have relative conductivities of 1.3, 4.3 and 3.3, while the 0 and +1 channels have negligible conductivities. For comparison, M2TM shows relative conductivities of 1.9, 5.5 and 0.4 for the +2, +3 and +4 tetrads. Thus, while the +3 channel still dominates the other charged states for proton conduction in M2(21–97), the +4 channel plays a more significant role than in M2TM, with ~75% of the proton conductivity of the +3 tetrad.

The higher pK_a's of His37 in longer M2 constructs also imply changes in the protonation and deprotonation kinetics. In proton-transfer reactions from water to imidazole, a typical pK_a of 6.9 for the imidazoles indicates a five-order-of-magnitude ratio between the second-order rate constant (k_{on}) for proton association with imidazole and the first-order rate constant (k_{off}) for proton dissociation from the imidazolium, since $K_a/K_w = k_{on}/k_{off}$, where K_w is the auto-ionization constant of water [44]. Diffusion-limited proton association has rate constants of $10^8 – 10^{10}$ $M^{-1}s^{-1}$, depending on whether the transfer occurs in bulk solution or in confined space [12]. In comparison, the proton dissociation rate constants, k_{off}, are several thousand times per second, and constitute the rate-limiting step in proton shuttling. Thus, the higher His37 pK_a's in M2(21–97) can be caused by a larger k_{on} or a smaller k_{off} or both.

While His37 is protonated at higher pH in the cytoplasmic-containing M2 than in M2TM, the ^{15}N spectra between pH 5 and 6 do not show well resolved exchange peaks that were seen in the M2TM spectra [17,22] (Fig. 6c, d). This apparent paradox can be understood. The exchange peaks at 213 ppm and 185 ppm in the M2TM spectra of both the wild type and S31N mutant correspond to exchange populations of 53% : 24% : 23% for the τ tautomer, π tautomer, and cationic histidine [22], respectively. The dominance of neutral histidines among the interconverting species makes the chemical-exchange peaks detectable, because the 250-ppm peak of the unprotonated ^{15}N moves the population-weighted average ^{15}N chemical shifts downfield, resolving them from the protonated ^{15}N chemical shifts. Thus, with increased cationic histidine contents in M2(21–97), there are not enough neutral His37 residues between pH 5 and 6 to make the average ^{15}N chemical shifts sufficiently separated from the cationic ^{15}N peaks. This suggests that such exchange peaks may be observable at higher pH. Indeed, the high-temperature pH 7.0 spectrum (Fig. 6b) shows a partially resolved ^{15}N peak at 185 ppm, which matches the Nε2 exchange peak frequency in S31N and wild-type M2TM (Fig. 7a, b). This suggests that chemical exchange might occur near neutral pH in the cytoplasmic-containing M2, although more definitive evidence would require the observation of an Nδ1 exchange peak in the spectrum.

In addition to the protein construct length, the lipid membrane also affects the protonation equilibria of His37. The 2D spectra of DMPC-bound M2 at pH 7.0 (Fig. 4b) show little neutral tautomer peaks, in contrast to the spectra of the VM+ bound protein. This is consistent with the previous finding that the addition of cholesterol and SM in the membrane lowers the His37 pK_a. For M2TM, the two highest pK_a's in DMPC/DMPG bilayers are 8.2 [19], while the corresponding values in the virus-mimetic membrane are 7.6 and 6.8 [17]. Thus, higher membrane fluidity facilitates His37 protonation.

Influence of the cytoplasmic domain on the backbone conformation of His37

The multiple Cα and Cβ chemical shifts of His37 indicate multiple His37 backbone conformations in M2(21–97). This polymorphism is unique to His37, since other labeled residues do not show peak multiplicity. By correlating the Cα and Cβ chemical shifts to the imidazole chemical shifts, we identified the sidechain structures associated with the various backbone conformations. The cat0, cat1 and cat4 peaks are unique to the cytoplasmic-containing M2 and absent in M2TM (Table 1). Based on their imidazole chemical shifts, we can assign cat0 to a neutral histidine, while cat1 and cat4 can be assigned to cationic

histidines. The large Cα and Cβ chemical shift differences for all three states indicate relatively ideal α-helical (φ, ψ) torsion angles, which differ from the non-ideal helical conformations of the τ and π tautomers. Thus, the cytoplasmic domain creates a more α-helical His37 backbone regardless of whether the imidazole is cationic or neutral. We attribute this increased helicity to the electrostatic interaction among the four cytoplasmic domains of the tetramer (Fig. 9b). With a net charge of −4.1 for the cytoplasmic domain at pH 7.0, the electrostatic repulsion should promote straighter and more tilted TM helices, thus creating a more ideal α-helical structure at His37.

Taken together, the chemical shift data strongly suggest that the cat0 to cat4 conformations correspond to His37 structures in increasingly charged tetrads. Due to intermolecular interactions among the four histidines, the backbone conformation for cationic histidine or for the τ or π tautomeric sidechains should not be unique. For example, the neutral τ tautomer in the presence of one or two cationic histidines (+1 and +2 tetrads) should exhibit a slightly different backbone conformation from a τ tautomer in a fully neutral tetrad (0 tetrad) due to the stronger electrostatic repulsion of the former. Similarly, a cationic histidine in the +3 tetrad would be expected to have a slightly different conformation from a cationic histidine in the presence of two neutral histidines and one other cationic histidine (+2 tetrad). To estimate the (φ, ψ) torsion angles of His37, we ran the TALOS+ program [45] using the His37 chemical shifts measured here and the Leu36 and Leu38 chemical shifts measured before in M2TM [42,46]. We make the approximation that the two neighboring leucine residues do not have significant chemical shift changes with pH. Fig. S5 shows the (φ , ψ) angles of the three neutral and four cationic His37 states, and compare them with the ideal (φ , ψ) angles of transmembrane α-helices and water-soluble α-helices [47,48]. It can be seen that the backbone conformations associated with the τ and π tautomers at high pH deviate the most from the ideal α-helical conformations. Among the four cationic states, the cat2 and cat4 conformations are the closest to the ideal TM α-helical conformation. The cat0 to cat4 torsion angles have relatively small uncertainties of 5° whereas the torsion angles predicted for the τ and π tautomers have larger uncertainties of 10° and 30° for φ and ψ, respectively, which are consistent with the non-ideal helical nature of these two conformations.

The His37 chemical shifts and pH dependence in M2(21-97) are generally consistent with those observed in M2TM and amino acid histidine, but differ significantly from the chemical shifts reported for M2CD. In DOPC/DOPE-bound M2(22–62), two sets of His37 chemical shifts were measured [29]. The main conformer has (Cγ, Cδ2, Cε1) chemical shifts of (135, 117, 134) ppm, while the minor conformer has chemical shifts of (129, 114, 135) ppm. Both sets were observed at both pH 7.5 and pH 6.0, thus their difference are not caused by pH. The major conformer can be assigned to a cationic histidine but the minor conformer's chemical shifts do not agree with the trends of any of the three histidine structures (Fig. 2a), and in the absence of any ^{15}N chemical shifts, the structure is unknown, thus no conclusion can be drawn about the nature of the two conformations. In another study of the related M2(18–60), two sets of His37 chemical shifts with similar intensities were found at pH 7.8 [26]. Both ^{13}C and ^{15}N chemical shifts were measured, which allowed the two states to be assigned to the τ tautomer. This τ tautomer sidechain is correlated with two (Cα, Cβ) cross peaks, one of which is the same as the cat0 peak in M2(21–97). Thus, one of the

high-pH His37 conformations in M2(18–60) and M2(21–97) are identical. However, in contrast to M2(21–97), M2(18–60) exhibits widespread peak doubling for many TM residues, indicating C_2 symmetry for the tetramer. Since the two histidine conformations are both present at high pH, this peak doubling cannot be attributed to imidazole-imidazolium dimer formation. Therefore, no evidence for an imidazole-imidazolium dimer has been found in any M2 constructs, and the C_2 symmetry is not observed in M2 constructs containing the full cytoplasmic domain.

Conclusion

The current SSNMR data indicate that the M2 cytoplasmic domain facilitates protonation of the transmembrane His37, giving rise to higher pK_a's than that of the TM peptide. We attribute the higher pK_a's to the acidic nature of the cytoplasmic domain, which may directly increase proton transfer rates from water to imidazole by electrostatic attraction or indirectly facilitate proton transfer by opening the TM pore at the His37 constriction. The measured His37 pK_a's suggest that protonation becomes more cooperative in the presence of part or whole of the cytoplasmic domain. pH-dependent Cα and Cβ chemical shifts indicate that as the four His37 residues are progressively protonated, they adopt many distinct conformations, which can be assigned to different charged tetrads due to intermolecular interactions. Compared to the TM peptide, the His37 backbone conformation is more α-helical in the presence of the cytoplasmic domain, indicating that electrostatic interactions among the four cytoplasmic tails order the four-helix bundle. These results provide a molecular basis for the higher proton conductance of full-length M2 compared to the TM peptide, and delineate the detailed effects of the cytoplasmic domain on the TM helix conformations.

Supplementary Material

Refer to Web version on PubMed Central for supplementary material.

Acknowledgments

References

1. Pinto LH, Holsinger LJ, Lamb RA. Cell. 1992; 69:517. [PubMed: 1374685]

2. Pinto LH, Lamb RA. J Biol Chem. 2006; 281:8997. [PubMed: 16407184]

3. Cady SD, Luo WB, Hu F, Hong M. Biochemistry. 2009; 48:7356. [PubMed: 19601584]

4. Rossman JS, Lamb RA. Virology. 2011; 411:229. [PubMed: 21237476]

5. Holsinger LJ, Lamb RA. Virology. 1991; 183:32. [PubMed: 2053285]

6. Liao S, Fritzsching K, Hong M. Protein Sci. 2013; 22:1623. [PubMed: 24023039]

7. Sharma M, Yi M, Dong H, Qin H, Peterson E, Busath D, Zhou HX, Cross TA. Science. 2010; 330:509. [PubMed: 20966252]

8. Zebedee SL, Richardson CD, Lamb RA. J Virol. 1985; 56:502. [PubMed: 3840537]

9. Lamb, RA.; Holsinger, KJ.; Pinto, LH. Cellular Receptors of Animal Viruses. Wemmer, E., editor. Cold Spring Harbor Lab Press; Plainview, NY: 1994. p. 303

10. Wang C, Lamb RA, Pinto LH. Biophys J. 1995; 69:1363. [PubMed: 8534806]

11. Balannik V, Carnevale V, Fiorin G, Levine BG, Lamb RA, Klein ML, Degrado WF, Pinto LH. Biochemistry. 2010; 49:696. [PubMed: 20028125]

12. Hong M, DeGrado WF. Protein Sci. 2012; 21:1620. [PubMed: 23001990]

13. Wang J, Qiu JX, Soto CS, DeGrado WF. Curr Opin Struct Biol. 2011; 21:68. [PubMed: 21247754]

14. Sansom MSP, Kerr ID, Smith GR, Son HS. Virology. 1997; 233:163. [PubMed: 9201226]

15. Chen H, Wu Y, Voth GA. Biophys J. 2007; 93:3470. [PubMed: 17693473]

16. Okada A, Miura T, Takeuchi H. Biochemistry. 2001; 40:6053. [PubMed: 11352741]

17. Hu F, Schmidt-Rohr K, Hong M. J Am Chem Soc. 2012; 134:3703. [PubMed: 21974716]

18. Pinto LH, Dieckmann GR, Gandhi CS, Papworth CG, Braman J, Shaughnessy MA, Lear JD, Lamb RA, DeGrado WF. Proc Natl Acad Sci USA. 1997; 94:11301. [PubMed: 9326604]

19. Hu J, Fu R, Nishimura K, Zhang L, Zhou HX, Busath DD, Vijayvergiya V, Cross TA. Proc Natl Acad Sci USA. 2006; 103:6865. [PubMed: 16632600]

20. Hong M, Fritzsching KJ, Williams JK. J Am Chem Soc. 2012; 134:14753. [PubMed: 22931093]

21. Hu F, Luo W, Hong M. Science. 2010; 330:505. [PubMed: 20966251]

22. Williams JK, Tietze D, Wang J, Wu Y, DeGrado WF, Hong M. J Am Chem Soc. 2013; 135:9885. [PubMed: 23758317]

23. Ma C, Polishchuk AL, Ohigashi Y, Stouffer AL, Schön A, Magavern E, Jing X, Lear JD, Freire E, Lamb RA, DeGrado WF, Pinto LH. Proc Natl Acad Sci USA. 2009; 106:12283. [PubMed: 19590009]

24. Nguyen PA, Soto CS, Polishchuk A, Caputo GA, Tatko CD, Ma C, Ohigashi Y, Pinto LH, DeGrado WF, Howard KP. Biochemistry. 2008; 47:9934. [PubMed: 18754675]

25. Tobler K, Kelly ML, Pinto LH, Lamb RA. J Virol. 1999; 73:9695. [PubMed: 10559278]

26. Andreas LB, Eddy MT, Chou JJ, Griffin RG. J Am Chem Soc. 2012; 134:7215. [PubMed: 22480220]

27. Andreas LB, Eddy MT, Pielak RM, Chou JJ, Griffin RG. J Am Chem Soc. 2010; 132:10958. [PubMed: 20698642]

28. Colvin MT, Andreas LB, Chou JJ, Griffin RG. Biochemistry. 2014; 53:5987. [PubMed: 25184631]

29. Can TV, Sharma M, Hung I, Gor'kov PL, Brey WW, Cross TA. J Am Chem Soc. 2012; 134:9022. [PubMed: 22616841]

30. Miao Y, Qin H, Fu R, Sharma M, Can TV, Hung I, Luca S, Gor'kov PL, Brey WW, Cross TA. Angew Chem Int Ed Engl. 2012; 51:8383. [PubMed: 22807290]

31. Cady SD, Wang T, Hong M. J Am Chem Soc. 2011; 133:11572. [PubMed: 21661724]

32. Hong M, Gross JD, Hu W, Griffin RG. J Magn Reson. 1998; 135:169. [PubMed: 9799691]

33. Hong M, Jakes K. J Biomol NMR. 1999; 14:71. [PubMed: 10382307]

34. Cady SD, Goodman C, Tatko C, DeGrado WF, Hong M. J Am Chem Soc. 2007; 129:5719. [PubMed: 17417850]

35. Morcombe CR, Zilm KW. J Magn Reson. 2003; 162:479. [PubMed: 12810033]

36. Roberts JE, Harbison GS, Munowitz MG, Herzfeld J, Griffin RG. J Am Chem Soc. 1987; 109:4163.

37. Hohwy M, Jakobsen HJ, Eden M, Levitt MH, Nielsen NC. J Chem Phys. 1998; 108:2686.

38. Takegoshi K, Nakamura S, Terao T. Chem Phys Lett. 2001; 344:631.

39. Li S, Hong M. J Am Chem Soc. 2011; 133:1534. [PubMed: 21207964]

40. Cheng F, Sun H, Zhang Y, Mukkamala D, Oldfield E. J Am Chem Soc. 2005; 127:12544. [PubMed: 16144402]

41. Vila JA, Arnautova YA, Vorobjev Y, Scheraga HA. Proc Natl Acad Sci U S A. 2011; 108:5602. [PubMed: 21422292]

42. Cady SD, Hong M. Proc Natl Acad Sci USA. 2008; 105:1483. [PubMed: 18230730]

43. Brelidze TI, Niu X, Magleby KL. Proc Natl Acad Sci U S A. 2003; 100:9017. [PubMed: 12843404]

44. Fersht, A. Enzyme structure and mechanism. 2. W.H. Freeman; New York: 1985.

45. Shen Y, Delaglio F, Cornilescu G, Bax A. J Biomol NMR. 2009; 44:213. [PubMed: 19548092]

46. Cady SD, Mishanina TV, Hong M. J Mol Biol. 2009; 385:1127. [PubMed: 19061899]

47. Kim S, Cross TA. Biophys J. 2002; 83:2084. [PubMed: 12324426]

48. Smith LJ, Bolin KA, Schwalbe H, MacArthur MW, Thornton JM, Dobson CM. J Mol Biol. 1996; 255:494. [PubMed: 8568893]

```
        21              31              41              51
SNA DSSDPLVVAA  SIIGILHLIL  WILDRLFFKS  IYRFFEQGLK
    RGPSTEGVPE  SMREEYRKEQ  QSAVDADDSQ  FVSIELE
    61              71              81              91
```

Figure 1.
Amino acid sequence of M2(21–97), in which His37 is the only histidine residue.
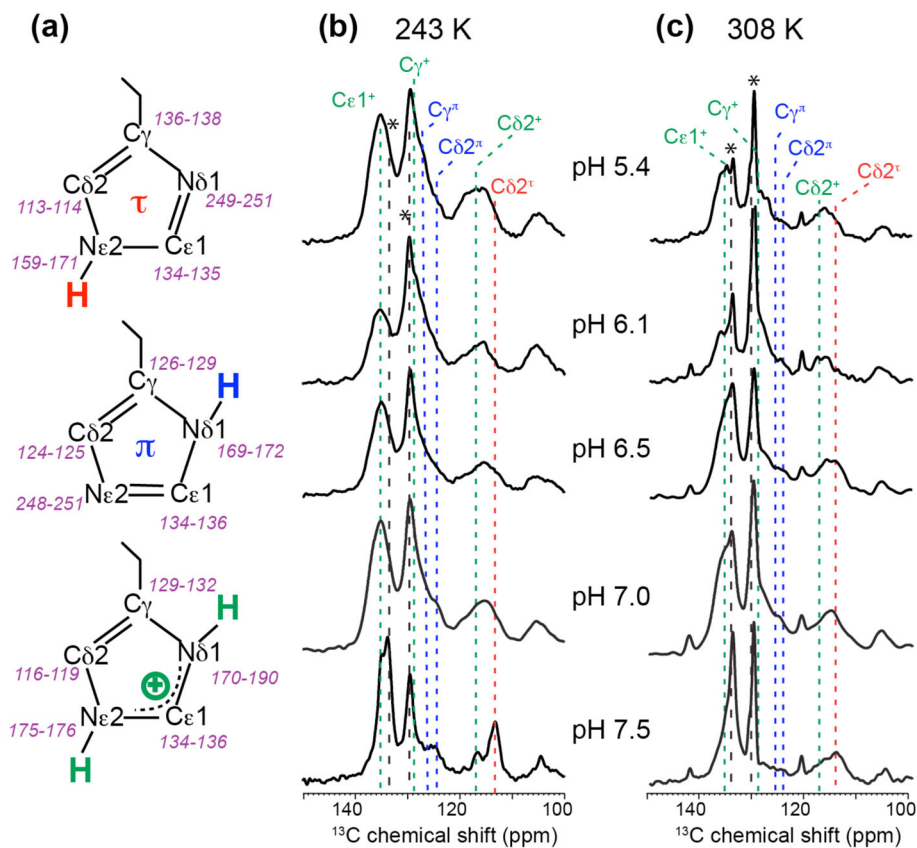
Figure 2.
(a) Chemical structures of the three forms of histidine and their characteristic chemical shift ranges. (b–c) Aromatic region of the ^{13}C CP-MAS spectra of His37 in VM+ bound M2(21–97) from pH 7.5 to 5.4. Peak assignments are shown in red for the τ tautomer, blue for the π tautomer and green for cationic histidine. Asterisks indicate the lipid natural-abundance ^{13}C peaks. (b) 243 K spectra. (c) 308 K spectra.
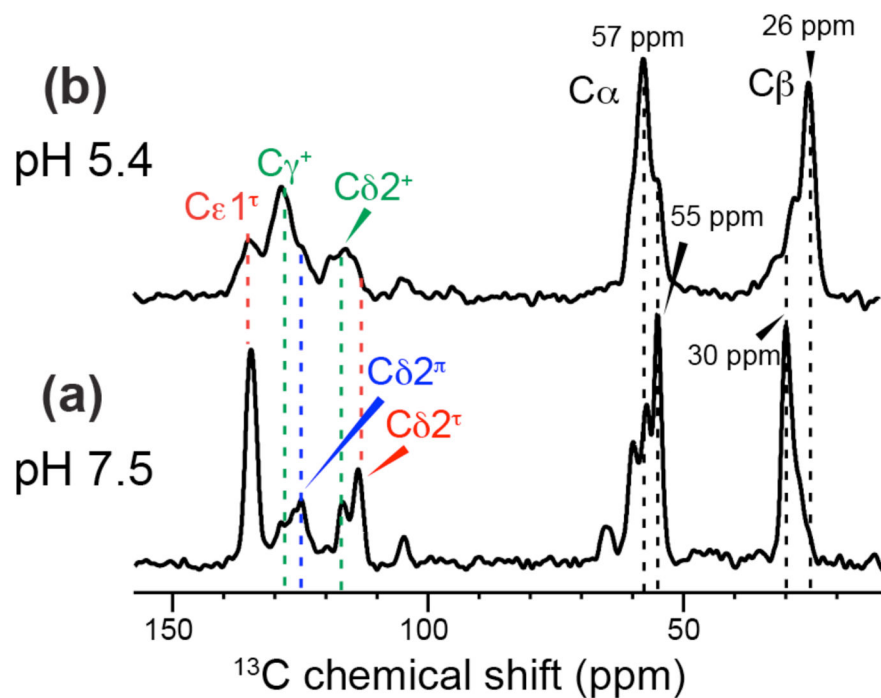
Figure 3.
DQ filtered ^{13}C spectra of His37 in VM+ bound M2(21–97) at 243 K. (a) pH 7.5. (b) pH 5.4. The pH 7.5 spectra are dominated by τ (red) and π (blue) tautomer signals, while the pH 5.4 spectra show mostly cationic His signals (green). Multiple Cα and Cβ chemical shifts are observed, and the low-pH state shows more downfield Cα chemical shifts and more upfield Cβ chemical shifts than the high-pH sample, indicating a more ideal helical conformation.
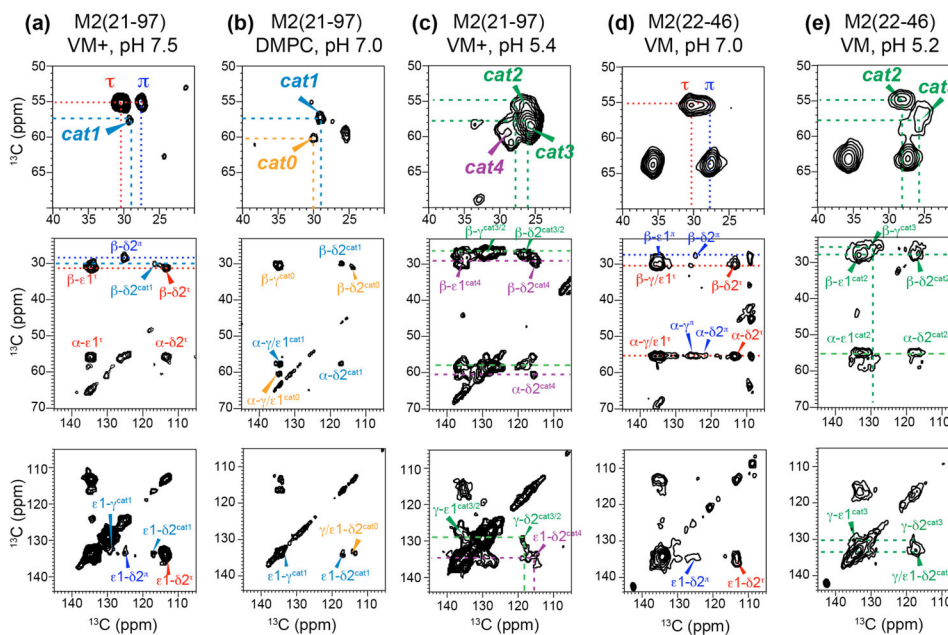
Figure 4.
2D ^{13}C-^{13}C correlation spectra of His37 in M2(21–97) and M2(22–46) at various pH and in different lipid membranes. (a) M2(21–97) in the VM+ membrane at pH 7.5. (b) M2(21–97) in the DMPC membrane at pH 7.0. (c) M2(21–97) in the VM+ membrane at pH 5.4. (d) M2(22–46) in the VM membrane at pH 7.0. (e) M2(22–46) in the VM membrane at pH 5.2. A total of seven backbone conformations are observed, manifested by seven distinct Cα–Cβ cross peaks. Correlation of these Cα–Cβ peaks to imidazole sidechain peaks allow the assignment of these conformations. Apart from the neutral τ and π tautomers, the other five states are denoted as cat0 to cat4. All spectra were measured between 243 and 253 K.
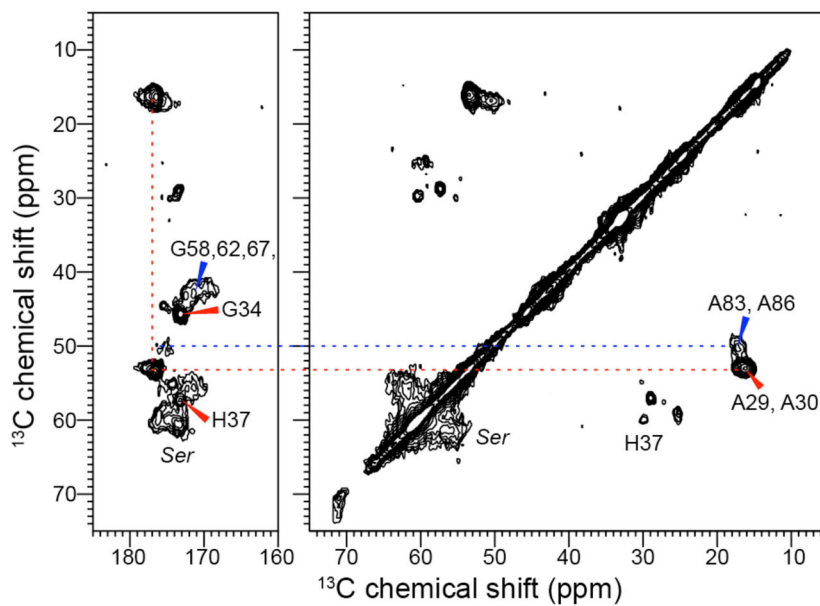
Figure 5.
2D ^{13}C PDSD spectrum of DMPC-bound M2(21–97), showing the cross peaks for His, Ala, Gly and Ser. The well-resolved Ala region does not show multiple peaks per residue, indicating that the His37 chemical shift multiplicity is specific to this residue due to its complex pH-dependent chemistry. The spectrum was measured with a 100 ms mixing time at 253 K on a 900 MHz spectrometer.
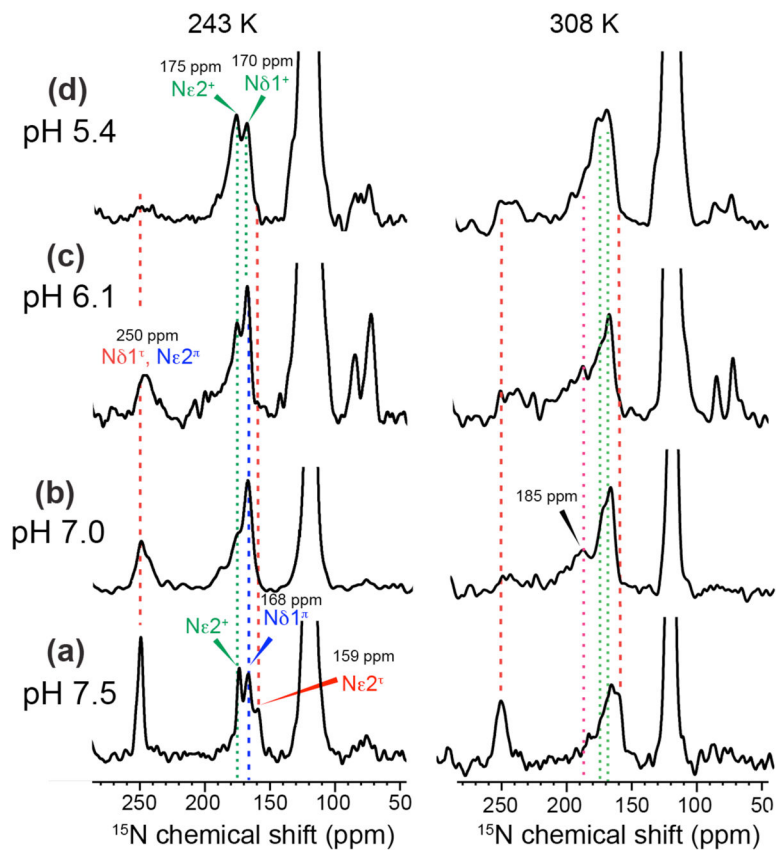
Figure 6.
[15]N CP-MAS spetra of His37 in VM+ bound M2(21–97) as a function of pH at 243 K and 308 K. (a) pH 7.5. (b) pH 7.0. (c) pH 6.1. (d) pH 5.4. The low-temperature spectra reveal the rigid-limit structure while the high-temperature spectra signify conformational dynamics and proton-exchange dynamics.
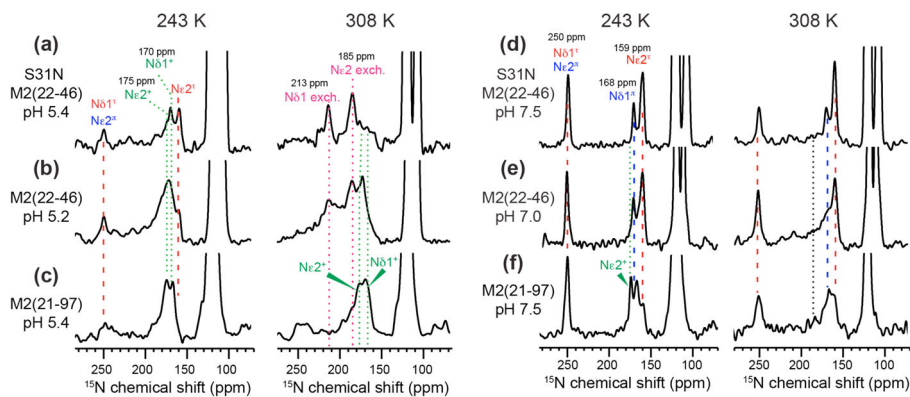
Figure 7.
Comparison of His37 ^{15}N spectra in M2(21–97) and M2(22–46) bound to virus-mimetic lipid membranes. (a) S31N M2(22–46) at pH 5.4. (b) Wild-type M2(22–46) at pH 5.2. (c) M2(21–97) at pH 5.4. (d) S31N M2(22–46) at pH 7.5. (e) Wild-type M2(22–46) at pH 7.0. (f) M2(21–97) at pH 7.5. Nδ1 and Nε2 exchange peaks are resolved in the low-pH spectra of M2(22–46) at 308 K, while M2(21–97) does not show such exchange peaks at similar pH. At high temperature, the M2(21–97) linewidths are larger than the M2TM linewidths, indicating increased conformational dynamics and proton exchange kinetics.
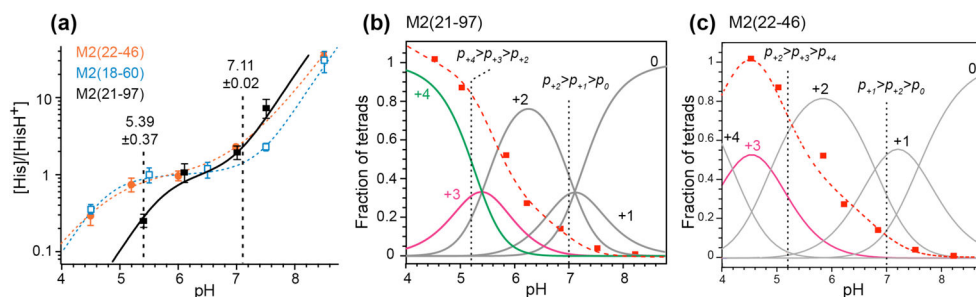
Figure 8.
pK$_a$ determination of His37 in M2(21–97). (a) Neutral-to-cationic histidine concentration ratio as a function of pH. M2(21–97) data (black) are overlaid with the previously reported M2(22–46) data (red) [17] and the M2(18–60) data [28]. The neutral histidine concentration in M2(21–97) shows a steeper decline with decreasing pH than the shorter M2 constructs. The two extracted pK$_a$'s are indicated by black dashed lines. (b) Fraction of charged tetrads of His37 in M2(21–97) as a function of pH. Because two pK$_a$'s are resolved, three charged states intercept at two pH values: the 0, +1 and +2 tetrads intercept at pH 7.1, while the +2, +3 and +4 tetrads intercept at pH 5.4. The +3 tetrad contributes the most to the proton current, followed closely by the +4 tetrad. Fitting the H$^+$ current of the Udorn strain of M2 as a function of pH [10] (red squares and red dashed line) constrains the relative single-channel conductivity of the different charged tetramers. (c) Previously reported tetrad populations of M2(22–46) as a function of pH. Four pK$_a$'s were obtained, and the +3 charged tetrad dominates the other charged states in contributing to the proton current. Black dotted lines in (b) and (c) indicate the different charged-state populations between the long and short M2 constructs at pH 7.0 and pH 5.2. The long M2 construct shows higher populations of the more cationic tetrads than the short M2 construct.
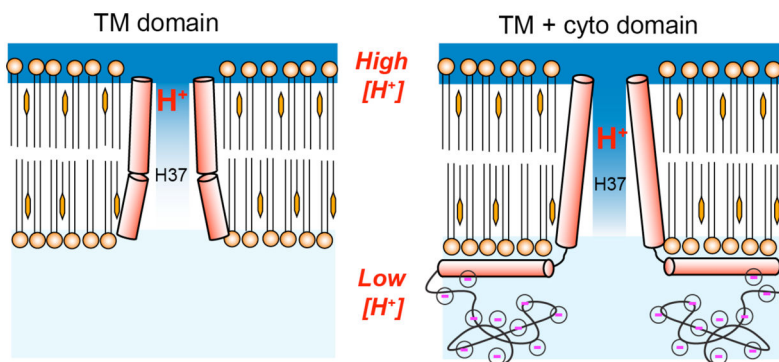
Figure 9.
Schematic model of His37-mediated proton conduction in cytoplasmic-containing M2. The M2 cytoplasmic domain, which contains a large number of acidic residues, facilitates proton conduction through electrostatic attraction, thus increasing the His37 pK_a's compared to the TM construct. The darker blue gradient on the right depicts higher proton concentrations in the channel. The His37 backbone is more α-helical in the longer M2 construct, which may result from electrostatic repulsion among the four negatively charged cytoplasmic domains. For clarity, only two of the four molecules of the tetrameric channel are depicted.

Table 1

^{13}C and ^{15}N chemical shifts (ppm) of resolved His37 structures in M2(21–97) and M2(22–46). All ^{13}C chemical shifts are referenced to TMS.

Site	τ tautomer	π tautomer	cat0	cat1	cat2	cat3	cat4
Cα	55	55	60	58	55	58	60
Cβ	30	28	30	29	29	26	29
(Cα,Cβ)^1	25	27	30	29	26	32	31
Cγ	136	125	-	133	135	129	133
Cδ2	114	124	114	117	118	118	117
(Cγ,Cδ2)^1	22	1	-	16	17	9	16
Cε1	135	135	134	134	134	136	134
Nδ1	250	168	-	-	-	-	-
Nε2	159	250	-	-	-	-	-
M2 constructs	22–46 21–97	22–46 21–97	- 21–97	- 21–97	22–46 21–97	22–46 21–97	- 21–97
pH	7.0–8.5	7.0–8.5	7.0–8.5	7.0–7.5	5.2	4.5–5.4	5.4
Sidechain structure	τ tautomer	π tautomer	τ tautomer	cationic	cationic	cationic	cationic

^{1}The chemical shift difference between Cα and Cβ and between Cγ and Cδ2 are shown in italics.

Table 2

Imidazole ^{15}N peak intensities and neutral versus cationic histidine concentrations in M2(21–97). For comparison, the concentration ratios of M2(18–60) [28] and M2(22–46) [17] based on previously published pK_a's are also listed.

pH	M2(21–97)			M2(18–60)	M2(22–46)
	I_{NH}/I_N	κ	[His]/[HisH$^+$]	[His]/[HisH$^+$]	[His]/[HisH$^+$]
5.4	14.0±2.4	1.60	0.26±0.05	0.87	0.79
6.1	4.16±0.73	1.48	1.10±0.30	1.00	1.12
7.0	2.61±0.26	1.30	1.99±0.39	1.30	2.28
7.5	1.86±0.11	1.47	7.54±2.12	2.28	4.70

Table 3

Comparison of His37 pK_a's in different M2 constructs bound to varying membranes.

M2	Phospholipid membranes	pK_a's	Average pK_a
M2(21–97)	POPC, POPE, SM, cholesterol	7.1, 5.4	6.3
M2(18–60) [28]	DPhPC	7.6, 4.5	6.1
M2(22–46) [17]	DPPC, DPPE, SM, cholesterol	7.6, 6.8, 4.9, 4.2	5.9
M2(22–46) [19]	DMPC, DMPG	8.2, 8.2, 6.3, < 5.0	< 6.9